Thin Solid Films **484** (2005) p 10– 17

Rhodium particles supported by thin vanadia films as model systems for catalysis: An electron microscopy study

S. Penner[a], D. Wang[b], R. Schlögl[b], K. Hayek[a,*]

[a]*Institut für Physikalische Chemie, Universität Innsbruck, Innrain 52a, A-6020 Innsbruck, Austria*
[b]*Fritz-Haber-Institut der Max-Planck-Gesellschaft, Faradayweg, 4-6, D-14195 Berlin, Germany*

Abstract

Well-shaped Rh particles grown epitaxially on NaCl surfaces were coated with a 25 nm layer of crystalline vanadium oxide by reactive deposition in 10^{-4} mbar oxygen. The Rh/VO_x film was subjected to consecutive heat treatments in 1 bar oxygen and in 1 bar hydrogen up to 673 K. The structural and morphological changes were monitored by (high-resolution) transmission electron microscopy, selected area electron diffraction and electron energy-loss spectroscopy and compared to the alterations of a bare vanadium oxide film treated under equal conditions. The stoichiometry and structure of the VO_x support depend on the temperature of the NaCl template and on the deposition rate. Low deposition rates and high substrate temperatures favour the generation of a pure V_2O_3 phase, with both V_2O_3 and the Rh particles in epitaxial relation to NaCl (001).

A treatment in 1 bar O_2 between 300 and 573 K converts the supporting oxide into mixed V_2O_3, VO_2 and V_2O_5 phases. Oxidation at 673 K induces a complete reconstruction into a single V_2O_5 phase, while an oxygen treatment at 723 K transforms also the Rh particles into (β)Rh_2O_3. Reduction of the bare V_2O_5 film in 1 bar hydrogen yields cubic VO at 673 K, but reduction of the Rh/V_2O_5 film leads to VO formation already at 473 K. Finally, a reduction of vanadia-supported Rh particles at and above 573 K results in the formation of Rh/V alloy structures.

Keywords: Transmission electron microscopy; Vanadium oxide; Electron energy loss spectroscopy; Catalysis

1. Introduction

Oxide-supported rhodium particles have found numerous applications in heterogeneous catalysis. Vanadia-promoted rhodium is a very efficient catalyst for redox reactions, and vanadium oxide is known to promote the CO hydrogenation towards alcohols and other oxygenates [1,2]. If the Rh/vanadia system is transformed into a highly reduced state, strong metal-support interaction occurs [3] and the selectivity to ethanol may be close to 100% [4].

The synergism of rhodium and vanadium oxide to steer a catalytic reaction has also been observed on so-called "inverse" supported catalysts. Submonolayers of vanadia on a Rh surface also promote the CO hydrogenation and change the selectivity from methane to longer hydrocarbons [5,6]. Some of the present authors could recently show that a reduction of the vanadia overlayers at elevated temperature has a crucial influence on both the surface composition and the catalytic activity of a polycrystalline Rh surface [7]. A reduction at 773 K and above converts the VO_x submonolayers into a chemically and thermally stable subsurface Rh/V alloy with characteristic catalytic properties [8,9].

While the structural and chemical changes upon high-temperature reduction can be conveniently studied on "inverse" model systems by using Surface Science techniques [10], information about the surface stoichiometry and microstructure of industrial supported Rh/vanadia catalysts is not easily obtained. (Ex situ) electron micro-

* Corresponding author. Tel.: +43 512 507 5062; fax: +43 512 507 2925.
E-mail address: konrad.hayek@uibk.ac.at (K. Hayek).

scopy and diffraction are among the most useful techniques, but for high-resolution imaging and microdiffraction a defined crystallographic orientation of the noble metal particles (which should not be too small in size) is almost a necessity. This can be accomplished with a model system of epitaxially grown Rh particles in contact with a vanadia promoter or support. These "thin film model catalysts" and their advantages in studies of microstructural changes have been described previously [11]. If the thickness of the supporting film is kept below about 25 nm, they are particularly suited for characterization by high-resolution electron microscopy and selected area electron diffraction. Due to the regular polyhedral habit of the Rh particles they provide a definite initial state, allowing an easier detection and a better understanding of the alterations during the subsequent oxidation or reduction treatment. In the present investigation we follow the structural changes of the Rh particles and of a supporting vanadia film as a function of treatments in oxygen and hydrogen up to 673 K and attempt a correlation to the results obtained on the "inverse" counterpart, i.e., on the vanadia covered rhodium foil.

2. Experimental details

Nanocrystalline Rh particles were prepared by electron-beam deposition of the metal on vacuum-cleaved NaCl surfaces at a base pressure of 10^{-4} Pa and a substrate temperature of 623 K. They were covered by a supporting layer of vanadium oxide (20–25 nm thick), obtained by reactive deposition of V metal in 10^{-2} Pa oxygen, again at 623 K. For comparison, a pure vanadia film of the same thickness was also prepared and investigated in parallel. After dissolving the NaCl in distilled water the films were mounted on gold grids for electron microscopy observations.

The pure vanadia film and the Rh/VO_x film were subjected to oxidative (1 bar O_2 for 1 h) and reductive (1 bar H_2 for 1 h) treatments in the temperature range between 373 and 673 K, either in a flow system or in a circulating batch reactor. The resulting changes in structure and morphology were followed by high-resolution transmission electron microscopy (HRTEM), selected area electron diffraction (SAED) and electron energy loss spectroscopy (EELS). The electron micrographs were taken with a ZEISS EM 10C and with a Philips CM 200 microscope equipped with a field emission gun and a Gatan imaging filter.

3. Results and discussion

3.1. The VO_x film, as grown and upon oxidation to 673 K

Fig. 1a shows a VO_x film on NaCl (001) deposited at room temperature (a), in comparison to a film deposited at 623 K (b), both at the same (low) deposition rate of 0.8 Å vanadium/s. Whereas the former consists of very small grains, the latter is composed of regularly shaped

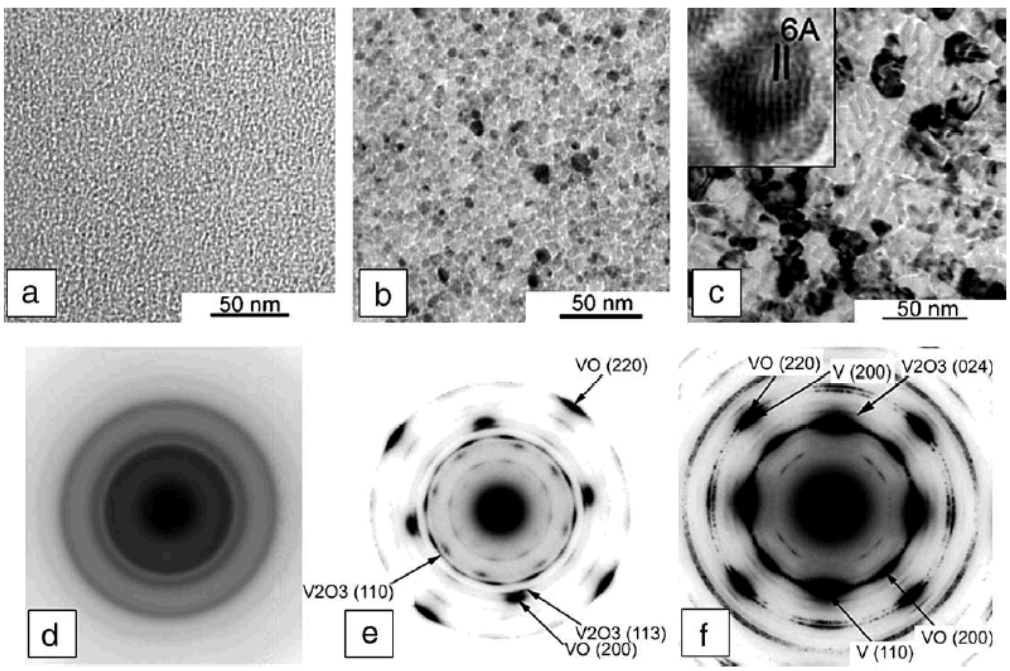

Fig. 1. Bare VO_x films deposited at room temperature (a) and at 623 K (b, c). Deposition rate: 0.8 Å V/s (a, b) and 12 Å V/s (c). The insert in (c) shows Moiré patterns due to overlapping VO and V lattices. The corresponding SAED patterns are shown in (d), (e) and (f).

crystallites (average grain size about 6 nm). Their difference is also revealed in the SAED patterns. The pattern arising from the low-temperature film (Fig. 1d) contains broad reflections and is typical for an almost amorphous structure. In contrast, the diffraction pattern of the high-temperature film (Fig. 1e) reveals a crystalline phase in orientational relation with the substrate. The broadening of the diffraction spots indicates that the grains are only partially ordered. Table 1 indicates that most of the reflections can be unambiguously assigned to rhombohedral V_2O_3 while the rest may be attributed to V_2O_3 but also to cubic VO which cannot be fully excluded. As seen in Fig. 1b, the electron micrographs of V_2O_3 films obtained at high temperature and low deposition rate are dominated by Bragg contrast. A (partially ordered) V_2O_3 phase is not only revealed by SAED (Fig. 1e) but also by HR-imaging. Fig. 2 shows several V_2O_3 grains in high resolution. Lattice fringes of 2.46 and 2.03Å can be distinguished arising from V_2O_3(110) [d_{theor}(110)=2.45 Å] and from V_2O_3 (202) [d_{theor}(202)=2.04 Å], respectively. These two lattice spacings correspond to intense reflections in the SAED pattern.

Fig. 1c shows a VO_x film deposited a high rate (12 Å V/s) at a substrate temperature of 623 K. Larger elongated grains (15–30 nm in size) are now observed. In the SAED pattern (Fig. 1f) reflections arising from fcc VO and from bcc V metal are detected besides those from V_2O_3, all in epitaxial relation to NaCl (001) (Table 1). Some weak reflections could not be assigned and may possibly arise from other substoichiometric phases. The VO grains grow mainly in their [001] zone axis, although weak reflections arising from a [011] axis (VO (111) and (311)) are also detected. Also the V particles exhibit both zone axes. The three components V_2O_3, VO and V metal are well-oriented with respect to each other. The composition and the crystallographic relations can also be deduced from a

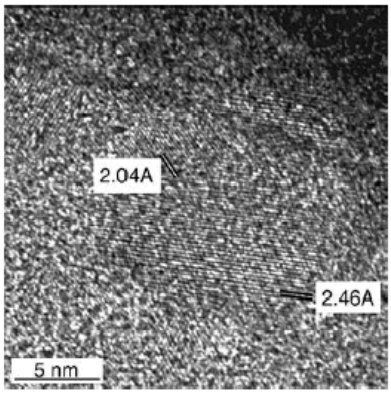

Fig. 2. High resolution detail of the V_2O_3 film shown in Fig. 1 (b).

number of Moiré patterns appearing in the "darker" domains, e.g., the fringes of about 6 Å shown in the insert of Fig. 1c arise from overlapping parallel VO (200) and V (200) spacings. They underline the ordered growth of V and VO in the relations VO [011]//NaCl [011] and VO (001)// NaCl (001), V [011]//NaCl [011] and V (001)//NaCl (001). Moiré patterns are only observed on the dark patches (Fig. 1c), thus suggesting that the darker domains correspond to V-rich areas.

Upon exposure to oxygen at 473 K for 1 h the electron image and diffraction are still characteristic of V_2O_3, and no considerable changes are observed compared to the as-grown state. Upon oxidation at 573 K the film starts to recrystallize and it undergoes a transformation into large elongated islands. The SAED patterns (not shown here) indicate the simultaneous presence of V_2O_3, VO_2 and V_2O_5. Increasing the oxidation temperature to 673 K leads to further significant changes of the microstructure. The low-magnification micrograph (Fig. 3a) shows oblong and sharp-edged crystals characteristic of V_2O_5. The SAED pattern (Fig. 3b and Table 1) matches the literature-reported

Table 1
Interplanar distances d_{hkl} [Å] measured on VO_x films deposited at 623 K at different rates, and possible correlation to rhombohedral V_2O_3, orthorhombic V_2O_5, fcc VO and bcc V metal (n.a.. . .not assigned)

V deposition rate: 0.8 Å V/s Substrate temperature 623 K			V deposition rate: 12 Å/s Substrate temperature 623 K			After oxidation 673 K, 1 h		
Assignment			Assignment			Assignment		
d (hkl)$_{exp}$	Lattice plane	d (hkl)$_{theor}$	d (hkl)$_{exp}$	Lattice plane	d (hkl)$_{theor}$	d (hkl)$_{exp}$	Lattice plane	d (hkl)$_{theor}$
3.63	V_2O_3 (012)	[3.65]	3.04	n.a.		5.75	V_2O_5 (200)	[5.74]
2.71	V_2O_3 (104)	[2.71]	2.36	VO (111)	[2.35]	4.41	V_2O_5 (010)	[4.36]
2.45	V_2O_3 (110)	[2.47]	2.13	V(110)	[2.14]	4.07	V_2O_5 (110)	[4.07]
2.17	V_2O_3 (113)	[2.19]	2.02	VO (200)	[2.03]	3.39	V_2O_5 (101)	[3.39]
2.04	V_2O_3 (202)	[2.05]	1.87	V_2O_3 (024)	[1.83]	2.91	V_2O_5 (400)	[2.87]
	VO (200)	[2.03]						
1.83	V_2O_3 (024)	[1.83]	1.69	V_2O_3 (116)	[1.70]	2.73	V_2O_5 (011)	[2.75]
1.69	V_2O_3 (116)	[1.70]	1.53	V (200)	[1.51]	2.61	V_2O_5 (301)	[2.60]
1.57	V_2O_3 (122)	[1.60]	1.47	VO (220)	[1.44]	2.46	V_2O_5 (211)	[2.48]
1.47	V_2O_3 (214)	[1.47]	1.37	n.a.		2.35	V_2O_5 (410)	[2.39]
	VO (200)	[1.44]	1.30	n.a.		2.16	V_2O_5 (020)	[2.18]
1.42	V_2O_3 (310)	[1.43]	1.25	V (211)	[1.24]	1.99	V_2O_5 (411)	[1.98]
			1.23	VO (311)	[1.22]			
			1.07	V (220)	[1.07]			

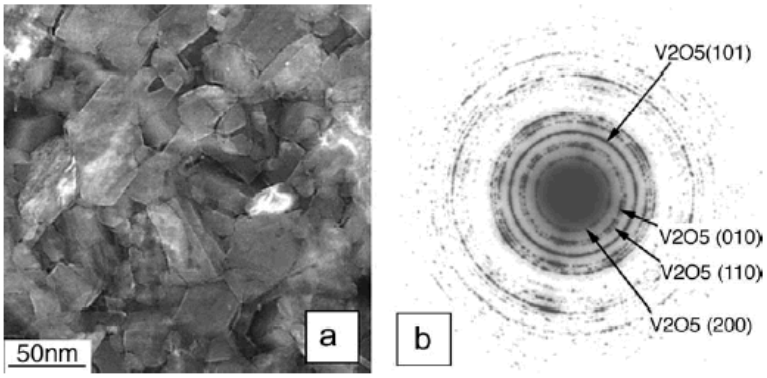

Fig. 3. Bare V_2O_3 film after oxidation at 673 K in 1 bar oxygen (a) and corresponding SAED pattern (b).

X-ray data of V_2O_5 [12]. Partial ordering with respect to the former NaCl substrate is still observed. In the HRTEM images (Fig. 4) lattice fringes of about 3.4 Å (Fig. 4a) and 4.1 Å (Fig. 4b) are observed, corresponding to V_2O_5 (101) [d_{theor}(101)=3.39 Å] and V_2O_5 (110) [d_{theor}(110)=4.07 Å], respectively.

3.2. The VO_x film after reduction up to 673 K

After oxidation to V_2O_5 at 673 K, a stepwise reduction was performed at increasing temperature, with the aim to obtain one uniform VO_x (x<2.5) phase. After reduction at 473 K and above the grain structure of V_2O_5 still persists in electron image and diffraction, but after reduction at 673 K the film attains a new "porous" structure in which the former vanadia grains can still be recognized (Fig. 5a). The diffraction pattern indicates cubic VO (Fig. 5b), and HRTEM reveals widespread lattice fringes of VO (2.04–2.07 Å, d_{200}(VO)=2.03 Å) (Fig. 6).

Additional information about the electronic structure of the newly formed VO-phase was obtained by EELS. It is known that the ratio of the V L_3/L_2 peak intensities increases with decreasing oxidation state of vanadium and that the intensity of the O pre-edge peak decreases with decreasing valence state of vanadium [13,14]. Hence it is reasonable to use these two features to characterise the oxidation state. Fig. 7 shows a set of high energy-loss spectra taken after several oxidation and reduction steps in comparison with the spectrum of the untreated V_2O_3 film. Each spectrum was first calibrated by the corresponding zero-loss spectrum, and then the background was subtracted and plural scattering was removed [15]. The spectra were compared with the EELS spectra of different V-oxides reported by Lin et al. [13]. The spectrum of the untreated sample (V_2O_3) and that obtained after oxidation at 673 K (V_2O_5) agree with the reported spectra with respect to the V L-edges and the near-edge structure of the O K-edge. In contrast, EELS spectra collected after oxidation at 573 K are consistent with the presence of a mixture of V-oxides. A shift of the V L-edges to higher energy losses, a change in the relative ratio of the V L_3/L_2 edges and a distinct change of the O K edge point to the presence of higher-oxidized vanadium states.

The change in the oxidation state of V after reduction at 673 K is confirmed by a shift of the V L-edges to lower energy loss compared to the sample oxidized at 673 K and by a change in their relative intensities. In addition, the O K-edge has changed its structure back to that expected for lower oxidized states.

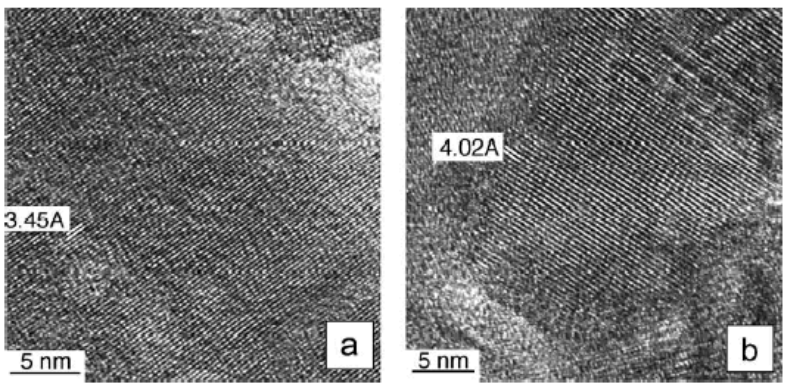

Fig. 4. HRTEM images of V_2O_5 grains exhibiting (101) (a) and (110) (b) lattice fringes.

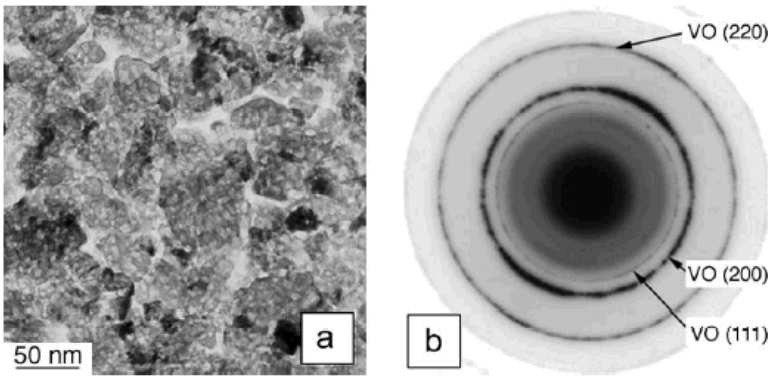

Fig. 5. V_2O_3 film after oxidation at 673 K and subsequent reduction at 673 K in 1 bar hydrogen (a), and corresponding SAED pattern (b).

3.3. The Rh/VO_x film as grown and after oxidation up to 723 K

Fig. 8a shows as-deposited Rh particles supported by V_2O_3 (nominal thickness of the deposited Rh film 1.8 nm, mean particle size 12 nm, thickness of the VO_x supporting layer 25 nm). The Rh particles exhibit square, rectangular and triangular shapes and can be well distinguished from the V_2O_3 support. Their three-dimensional habit was determined earlier by HREM and weak-beam dark field imaging to be mainly half-octahedral and half-tetrahedral [11]. The electron diffraction (Fig. 8b and Table 2) is a superposition of the V_2O_3 and the Rh patterns. It indicates perfect epitaxial growth of the Rh particles and a partial ordering of the V_2O_3 grains on the former NaCl (001) template.

After oxidation at 473 K the microstructure of the Rh/vanadia film is unchanged compared to the as-grown state and the SAED pattern shows well-oriented Rh particles and a uniform V_2O_3 phase. The absence of extra reflections shows that no interaction between Rh and V_2O_3 has taken place. Raising the oxidation temperature to 573 K causes a slight sintering of the V_2O_3 support and a closing of the grain boundaries (Fig. 9a). As expected from the behaviour of the corresponding Rh/Al_2O_3 system studied previously [16], the Rh particles keep their regular outlines and their shape remains almost unaffected. First signs of orientational disorder are indicated by the appearance of Rh (111) reflections in the diffraction pattern (Fig. 9c). However, at the same time the support changes its composition, similarly as the bare V_2O_3 film. Additional reflections in the SAED pattern are attributable to monoclinic VO_2 ($d_{-111}(VO_2)$=3.31 Å and $d_{011}(VO_2)$= 3.20 Å, Table 2). The VO_2 phase appears partially ordered in electron diffraction.

Similarly as observed on the bare vanadia film, a further increase of the oxidation temperature to 673 K results in the reconstruction into large V_2O_5 grains supporting the noble metal particles. The Rh particles are not affected by this transformation of the support and keep their rectangular and square outlines (Fig. 9b). The SAED pattern (Fig. 9d) and the V_2O_5(200) lattice spacings observed at high resolution (5.74 Å, insert in Fig. 9b) both reveal a uniform V_2O_5 phase.

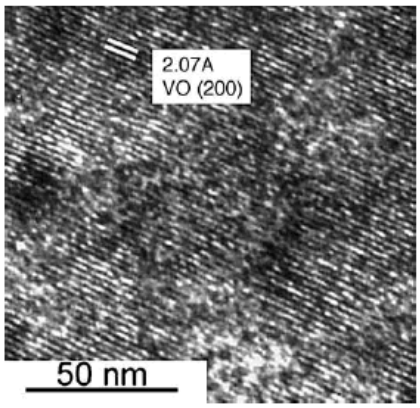

Fig. 6. VO (200) lattice fringes observed after oxidation at 673 K followed by reduction in 1 bar hydrogen at 673 K.

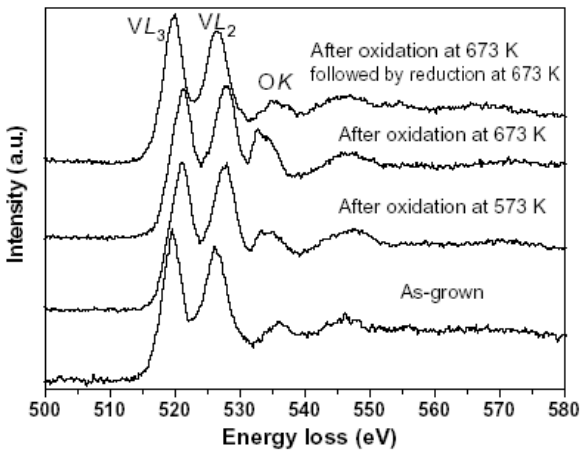

Fig. 7. EELS spectra of the bare V_2O_3 film after various oxidation and reduction steps.

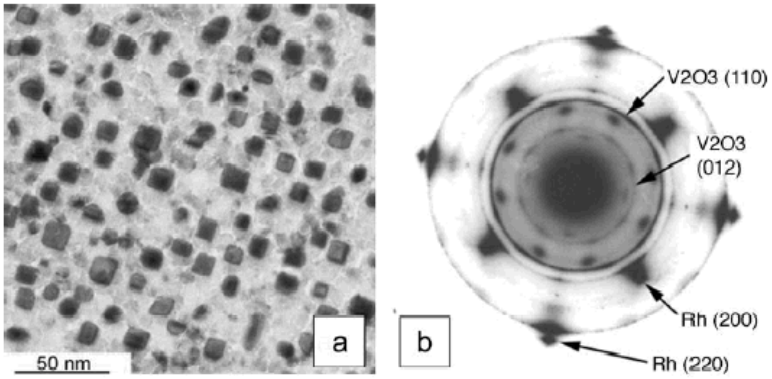

Fig. 8. As-grown Rh/V_2O_3 film (a) and SAED pattern (b). Mean Rh particle size 12 nm.

After oxidation at 723 K the appearance of the vanadia support is unchanged, but the Rh particles are now surrounded by a shell of β-Rh_2O_3, in analogy to the observations made by Rupprechter et al. [16] after oxidation of a corresponding Rh/Al_2O_3 system at the same temperature (not shown here). In conclusion, the changes in the support during oxidation can be considered as independent of the presence of Rh particles and vice versa.

3.4. The Rh/VO_x film after reduction up to 673 K

Subsequent to the oxidation at 673 K, a series of reduction treatments was performed on the Rh/vanadia system. A reduction *below* 473 K leaves the microstructure unchanged and the SAED pattern consists of rings from V_2O_5 and of broadened spots from fcc Rh, revealing that most Rh particles are still in their [110] zone axis. However, a reduction at 473 K induces significant structural alterations particularly of the support (Fig. 10a). Although the shape of the former V_2O_5 grains is still recognized, the support appears porous, similar to the bare VO_x film after reduction at *673 K*. The SAED pattern (Fig. 10d) reveals cubic VO. Obviously the Rh particles catalyze the reduction of V_2O_5 to lower oxidation states. The Rh particles keep their regular outlines, but appear to be enclosed by the reduced support (Fig. 10a).

A further reduction at 573 K does not change the appearance of the particles or the supporting oxide in the electron micrograph (Fig. 10b), but a number of new reflections appear in the diffraction pattern that may be attributed to alloy formation between rhodium and vanadium (Fig. 10e and Table 3). The entire pattern can be interpreted as a superposition arising from i) (001) oriented Rh particles, ii) a slightly ordered VO support, and iii) an orthorhombic Rh_5V_3 phase in good epitaxial relation with the Rh particles.

Further raising the reduction temperature results in an apparent enlargement of the metal particles on the electron micrograph and to a loss of particle ordering (shown in Fig. 10c for T_{red}=673 K). At the same time a large number of partly new ring reflections appear in the diffraction

Table 2
Interplanar distances d_{hkl} [Å] measured on Rh/VO_x as-grown and after oxidation at 573, and 673 K and possible correlation to rhombohedral V_2O_3, monoclinic VO_2, orthorhombic V_2O_5 and fcc Rh (n.a. . . .not assigned)

Rh/VO_x as-grown			Rh/VO_x after oxidation at 573 K			Rh/VO_x after oxidation at 673 K		
Assignment			Assignment			Assignment		
d (hkl)$_{exp}$	Lattice plane	d (hkl)$_{theor}$	d (hkl)$_{exp}$	Lattice plane	d (hkl)$_{theor}$	d (hkl)$_{exp}$	Lattice plane	d(hkl)$_{theor}$
4.26	n.a.		3.36	VO_2 (−111)	[3.31]	5.73	V_2O_5 (200)	[5.74]
3.62	V_2O_3 (012)	[3.66]	3.14	VO_2 (011)	[3.20]	4.36	V_2O_5 (010)	[4.36]
2.74	V_2O_3 (104)	[2.71]	2.44	V_2O_3 (110)	[2.48]	3.38	V_2O_5 (101)	[3.39]
2.44	V_2O_3 (110)	[2.48]	2.18	Rh (111)	[2.19]	2.88	V_2O_5 (400)	[2.87]
2.18	V_2O_3 (113)	[2.18]	2.09	V_2O_3 (202)	[2.05]	2.61	V_2O_5 (301)	[2.60]
2.05	V_2O_3 (202)	[2.05]	1.89	Rh (200)	[1.89]	2.46	V_2O_5 (211)	[2.48]
1.89	Rh (200)	[1.89]	1.81	V_2O_3 (024)	[1.82]	2.36	V_2O_5 (410)	[2.39]
1.79	V_2O_3 (024)	[1.83]	1.63	VO_2 (211)	[1.65]	2.17	Rh (111)	[2.19]
1.68	V_2O_3 (116)	[1.70]	1.41	V_2O_3 (300)	[1.43]	1.89	Rh (200)	[1.89]
1.47	V_2O_3 (214)	[1.47]	1.34	Rh (220)	[1.34]	1.76	V_2O_5 (002)	[1.78]
1.43	V_2O_3 (300)	[1.43]				1.50	V_2O_5 (701)	[1.48]
1.34	Rh (220)	[1.34]				1.34	Rh (220)	[1.34]
1.24	V_2O_3 (220)	[1.24]						

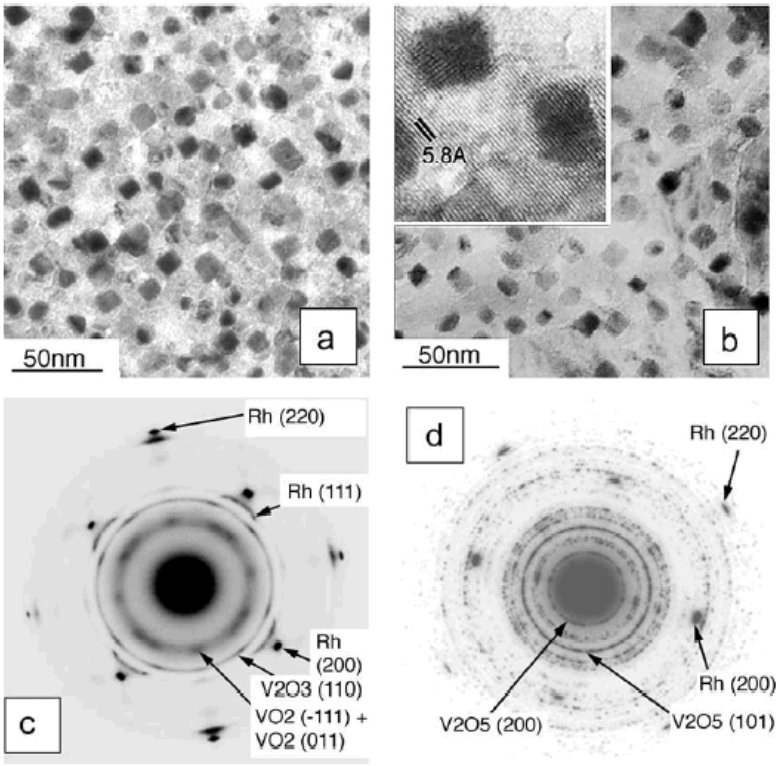

Fig. 9. Rh/V_2O_3 film after oxidation at 573 K (a) and 673 K (b). The insert in (b) shows V_2O_5 (200) lattice fringes. SAED patterns are shown in (c) and (d).

pattern (Fig. 10f and Table 3) which can be assigned to the vanadium suboxides VO and V_2O and to the alloy Rh_5V_3, but at this temperature other Rh–V alloys, particularly Rh_3V, cannot be excluded. Since metallic Rh was not detected it must be concluded that a treatment in 1 bar hydrogen at 673 K for 1h is sufficient to complete the

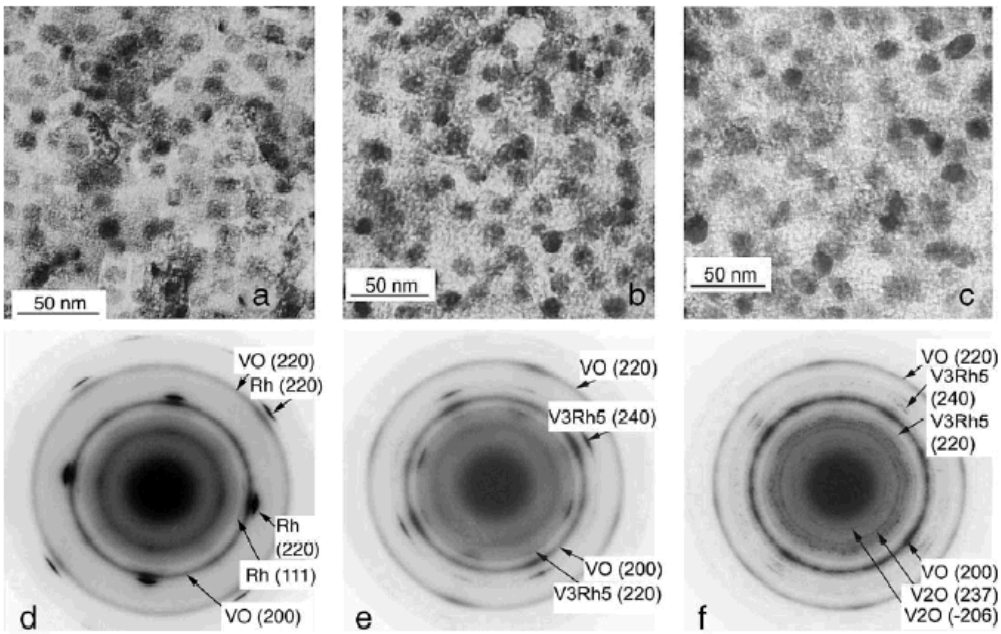

Fig. 10. Rh/V_2O_3 film after oxidation at 673 K followed by reduction in 1 bar hydrogen at 473 K (a), 573 K (b) and 673 K (c). Corresponding SAED patterns in (d–f).

Table 3
Interplanar distances d_{hkl} [Å] measured on Rh/VO_x after reduction at 573 and 673 K, and possible correlation to cubic VO, monoclinic V_2O, VO/V_2O with unknown crystal structure (ui) [15], cubic VRh_3 and orthorhombic V_3Rh_5

Rh/VO_x after reduction at 573 K			Rh/VO_x after reduction at 673 K		
Assignment			Assignment		
d (hkl)$_{exp}$	Lattice plane	d (hkl)$_{theor}$	d (hkl)$_{exp}$	Lattice plane	d d(hkl)$_{theor}$
2.31	V_3Rh_5 (220)	[2.34]	3.94	V_2O (−206)	[3.88]
2.03	VO (200)	[2.03]	3.05	V_2O (237)	[3.02]
1.76	V_3Rh_5 (240)	[1.76]	2.76	V_2O (271)	[2.79]
				V_3Rh_5 (200)	[2.71]
				V_2O, VO ui	[2.70]
					[2.71]
1.42	VO (220)	[1.43]	2.56	V_2O (464)	[2.58]
			2.49	V_2O, VO ui	[2.47]
					[2.48]
			2.34	V_3Rh_5 (220)	[2.34]
			2.14	V_3Rh_5 (002)	[2.16]
				VRh_3 (111)	[2.17]
				V_2O, VO ui	[2.16]
					[2.18]
			2.03	VO (200)	[2.03]
			1.93	V_3Rh_5 ui	[1.92]
			1.89	V_2O (578)	[1.89]
				VRh_3 (200)	[1.89]
			1.76	V_3Rh_5 (240)	[1.76]
			1.70	V_3Rh_5 (202)	[1.69]
				V_2O, VO ui	[1.68]
					[1.69]
			1.64	V_3Rh_5 (241)	[1.63]
				V_2O (3 7 12)	[1.65]
			1.43	VO (220)	[1.43]

alloy formation on this particular Rh/VO_x system with Rh particles of 10–15 nm in size. Larger Rh particles will require a significantly higher reduction temperature (up to 873 K) to be transformed into the alloy state.

If we compare this behaviour to that of a corresponding inverse catalyst—a VO_x submonolayer on a Rh foil [7,8]—we remember that a reduction in 100 mbar hydrogen induces the formation of the subsurface alloy at 773 K and above, which is in good qualitative agreement with our present observations. It is, however, of interest to note that a reduction at 573–623 K leads the present system into an intermediate state with a thin alloy phase (Rh_5V_3) in *topotactic* relation to the Rh particles. This state may be a starting point for an investigation of catalytic properties which may be comparable to those of the subsurface Rh/V alloy on the inverse Rh catalyst.

The resulting Rh/V alloys are surprisingly stable in air and oxygen. They obviously survive the transfer to the electron microscope, and an oxidation at 1 bar above 573 K is necessary to destroy the alloy structure completely.

4. Conclusions

The structure and composition of the pure vanadium film depend on the deposition rate (in 10^{-4} mbar oxygen) and on the temperature of the NaCl template. Low deposition rates and high substrate temperatures favour the generation of a pure V_2O_3 phase partly in epitaxial relation to NaCl (001). A treatment in 1 bar O_2 between 300 and 573 K converts the supporting oxide into mixed V_2O_3, VO_2 and V_2O_5 phases. Oxidation at 673 K induces a complete reconstruction into a uniform V_2O_5 phase. Reduction of the bare V_2O_5 film in 1 bar hydrogen yields cubic VO at 673 K.

The Rh/VO_x film was subjected to consecutive heat treatments in 1 bar oxygen and in 1 bar hydrogen up to 673 K. The as-grown Rh/vanadia catalyst is characterized by partial epitaxial relationships between the Rh particles and the VO/V_2O_3 support. A 1 bar oxygen treatment transforms the support into V_2O_5 at 673 K and the Rh particles into β-Rh_2O_3 at 723 K. A reduction of the Rh/V_2O_5 film at 473 K produces VO. Finally, the reduction of vanadia-supported Rh particles at and above 573 K results in the formation of Rh/V alloy structures with Rh_5V_3 as the most prominent one. This finding agrees at least qualitatively with the formation of subsurface alloys observed on single crystal and polycrystalline surfaces and offers a perspective for future applications in catalysis.

Acknowledgement

We thank the Austrian Science Fund for support under Project S 8105.

References

[1] M. Ichikawa, K. Shikakura, in: T. Seijama, K. Tanabe (Eds.), Proceedings of the 7th Int. Congress on Catalysis, Kondansha, Tokyo, 1980, p. 1468.
[2] J. Kowalski, G. van der Lee, V. Ponec, Appl. Catal. 19 (1985) 423.
[3] S.J. Tauster, S.C. Fung, R.L. Garten, J. Am. Chem. Soc. 100 (1978) 170.
[4] H.J. Luo, A.G.T.M. Bastein, A.A.J.P. Mulder, V. Ponec, Appl. Catal. 38 (1988) 241.
[5] A.B. Boffa, C. Lin, A.T. Bell, G.A. Somorjai, Catal. Lett. 27 (1994) 243.
[6] T. Hartmann, H. Knözinger, Z. Phys. Chem. 197 (1996) 113.
[7] W. Reichl, K. Hayek, J. Catal. 208 (2002) 422.
[8] W. Reichl, K. Hayek, Surf. Sci. 537 (2003) 247.
[9] W. Reichl, K. Hayek, J. Catal. 222 (2004) 53.
[10] K. Hayek, B. Jenewein, B. Klötzer, W. Reichl, Top. Catal. 13 (2000) 55.
[11] G. Rupprechter, K. Hayek, L. Rendón, M.J. Yacamán, Thin Solid Films 260 (1995) 148.
[12] Powder Diffraction File, International Center for Diffraction Data 1994, PDF Series 2 Sets 1–47.
[13] X.W. Lin, Y.Y. Wang, V.P. Dravid, P.M. Michalakos, M.C. Kung, Phys. Rev., B 47 (1993) 3477.
[14] D.S. Su, R. Schlögl, Catal. Lett. 83 (2002) 115.
[15] R.F. Egerton, Electron energy loss spectroscopy in the electron microscope, Plenum, New York, 1986.
[16] G. Rupprechter, K. Hayek, H. Hofmeister, J. Catal. 173 (1998) 409.